*Exploration Geophysics (2005) **36**, 181–188*

The Total Field Magnetometric Resistivity (TFMMR) Method Part I: theory and 2.5D forward modelling

Nader Fathianpour[1] **Graham Heinson**[2] **Antony White**[3]

Key Words: SAM, TFMMR, MMR, Biot-Savart law, analytical modelling, finite element modelling

ABSTRACT

The Sub-Audio Magnetics (SAM) method is a high-resolution electrical technique that derives information on sub-surface electrical and magnetic properties by introducing an electric current into the ground and measuring the total magnetic field changes on the Earth surface at a sub-metre interval via an optically pumped magnetometer. One parameter that may be derived from any SAM survey is the total-field magnetometric resistivity (TFMMR). To date, there are few quantitative interpretational schemes for deriving resistivity from TFMMR data. This paper outlines the theory to calculate the 2.5 dimensional (2.5D) TFMMR response due to a point source of current in an otherwise two-dimensional (2D) Earth. The problem is formulated in the wavenumber domain by first solving for the electrical potential from the current source, and then deriving orthogonal horizontal and vertical components of magnetic field using the modified Biot-Savart Law. An inverse Fourier transform is then applied to yield vector magnetic field components in the spatial domain, and hence the scalar TFMMR response.

A 2.5D finite-element modelling approach is developed to model TFMMR responses from various resistivity structures. For an isotropic, uniform resistivity Earth the finite-element model gives good agreement with analytical results, with an accuracy of about 4% in each of the three vector components. The greatest error is for the horizontal magnetic field component along strike. Finally, we demonstrate that the TFMMR technique is very useful for defining basement structures in areas of conductive regolith cover. The presence of a regolith (10 Ω.m) has little effect on the TFMMR responses provided that its thickness is less than about one twentieth of the current-electrode separation. Thus, for a typical electrode separation of 1.2 km, the TFMMR response is sensitive to basement structures for regolith thickness of up to 60 m, and hence is an important geophysical method for exploration beneath cover.

INTRODUCTION

The geophysical basis of the SAM exploration method has been fully described by Cattach et al. (1994), Cattach (1996), Fathianpour and Cattach (1995), and Boggs et al. (1998, 1999). It is a high-definition technique for simultaneously mapping electrical and magnetic properties of the ground. A time-varying (typically square-wave) electric current is applied to the ground in the sub-audio frequency range (5–20 Hz), between two distant electrodes. In general, any electrode configurations may be used in a SAM survey, but the most efficient layout currently used is the gradient array, or horseshoe layout (as shown in Figure 1). The reason for this is mainly due to the logistical ease and efficiency in data collection with the benefit of a higher signal-to-noise ratio by having the electrode wires at a reasonable distance from the edge of the survey area.

An optically pumped magnetometer, such as the TM-4 (Stanley and Cattach, 1996), is used to map the combination of Earth's static magnetic field with the artificially produced magnetic field from the galvanic current flow. Because the magnetic survey can be carried out rapidly on foot (traversing up to 20 km a day) at a sample rate of up to 400 Hz, sample spacing may be as small as 5 cm, although 0.2 to 0.5 m intervals are commonly used for geotechnical or mineral exploration applications. Line-spacings are typically a few metres to tens of metres, depending on the size of the target body.

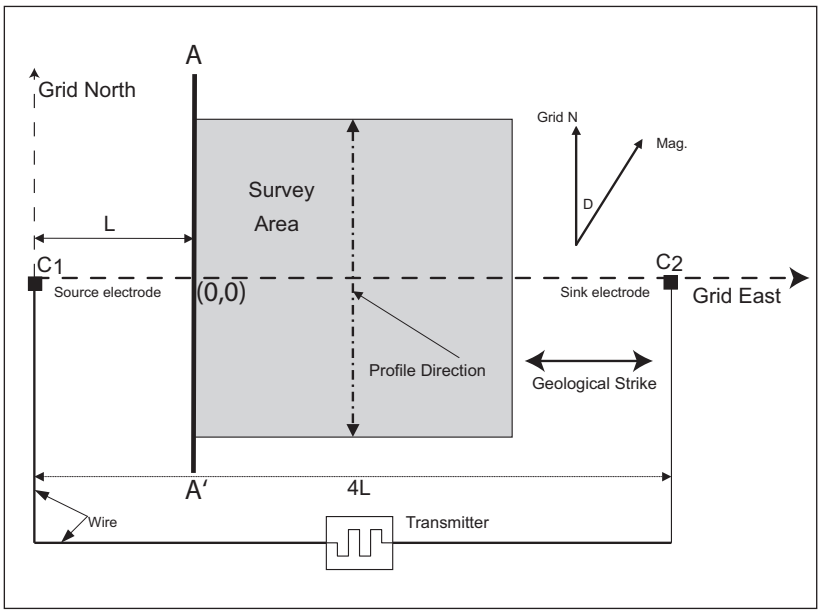

Fig. 1. Typical gradient array layout used in a SAM survey. Current electrodes C_1 and C_2 are optimally located along the direction of geological strike. Line A-A′ shows the location of the 2.5D model profiles in Figures 4, 5, and 6. map of the SAM survey results.

[1] *Department of Mining Engineering*
Isfahan University of Technology
Isfahan 84154, Iran
Phone: +98 311 391 5130
Facsimile: +98 311 391 2776
Email: fathian@cc.iut.ac.ir

[2] *Co-operative Research Centre for Landscapes*
Environment and Mineral Exploration
School of Earth and Environmental Sciences
University of Adelaide
Adelaide SA 5005, Australia

[3] *School of Chemistry, Physics and Earth Sciences*
Flinders University of South Australia
Bedford Park SA 5042, Australia

Manuscript received 6 August, 2004.
Revised manuscript received 13 April, 2005.

Spectral analysis of the observed magnetic fields yields the following SAM geophysical responses: (i) total magnetic intensity (TMI), (ii) total-field magnetometric resistivity (TFMMR), and (iii) total-field magnetometric induced polarisation (TFMMIP). This paper will discuss only the TFMMR part of the SAM response. To date, there have been few quantitative interpretational schemes for deriving electrical information from TFMMR data. This paper outlines the theory of the 2.5D TFMMR response due to a finite point source in a 2D Earth, and derives finite-element numerical responses for simple bodies that are compared to analytical expressions given by Fathianpour and Cattach (1995). Finally, we discuss the application of the TFMMR method for mineral exploration beneath conductive regolith cover.

BACKGROUND THEORY

Biot Savart Law

From Maxwell's equations, the resulting magnetic field **B** at location **r** due to a current density element **J** at location **r'** is given by the Biot Savart Law:

$$\mathbf{B}(r) = \frac{\mu_0}{4\pi}\int_V \frac{(\mathbf{r}-\mathbf{r}')\times\mathbf{J}(\mathbf{r}')}{|\mathbf{r}-\mathbf{r}'|^3}\,\mathrm{dv}' \ , \tag{1}$$

where v is the volume of space in which current density elements **J** are defined (Edwards, 1974; Edwards et al., 1978; Edwards and Nabighian, 1991). We assume that magnetic permeability of Earth materials is constant and equal to that of free space μ_0. We note that the current is the sole generator of the static magnetic field, and the distribution of this generator is characterised by the magnitude and direction of current density vector **J**.

In its general form, evaluation of equation (1) involves a knowledge and integration of the current density vector over the entire domain of the problem, which may be a computationally intensive task. Edwards et al. (1978) derived a more efficient formula, known as the modified Biot-Savart law, to calculate the total magnetic field as:

$$\mathbf{B}(\mathbf{r}) = \frac{\mu_0}{4\pi}\int_V \frac{\nabla'\phi(\mathbf{r}')\times\nabla'\sigma(\mathbf{r}')}{|\mathbf{r}-\mathbf{r}'|}\,\mathrm{dv}' \ , \tag{2}$$

where ϕ is the electric potential, σ is the electrical conductivity, and

$$\mathbf{J}(\mathbf{r}') = -\sigma(\mathbf{r}')\,\nabla'\,\phi(\mathbf{r}') \ . \tag{3}$$

As discussed by Edwards et al. (1978) and Fathianpour and Cattach (1995), this is a very useful expression for computing all three components of the magnetic field, as it reduces the integral just to surfaces of the inhomogeneities where $\nabla'\sigma(\mathbf{r}')$ is non-zero.

In computing the TFMMR response for any 2D geological model, three orthogonal components of magnetic field are required. In Cartesian co-ordinates, these components are obtained by expanding equation (2) and observing that for a 2D structure striking in the y-direction $\partial\,\sigma\,(x,\,z)/\partial\,y = 0$, so that

$$B_x(\mathbf{r}) = \frac{\mu_0}{4\pi}\int_V \frac{\left(\dfrac{\partial\,\sigma(x',z')}{\partial z'}\dfrac{\partial\phi(\mathbf{r}')}{\partial y'}\right)}{|\mathbf{r}-\mathbf{r}'|}dv' \ , \tag{4}$$

$$B_y(\mathbf{r}) = \frac{\mu_0}{4\pi}\int_V \frac{\left(\dfrac{\partial\,\sigma(x',z')}{\partial x'}\dfrac{\partial\,\phi(\mathbf{r}')}{\partial z'} - \dfrac{\partial\,\sigma(x',z')}{\partial z'}\dfrac{\partial\,\phi(\mathbf{r}')}{\partial x'}\right)}{|\mathbf{r}-\mathbf{r}'|}dv' \ , \tag{5}$$

and

$$B_z(\mathbf{r}) = -\frac{\mu_0}{4\pi}\int_V \frac{\left(\dfrac{\partial\,\sigma(x',z')}{\partial x'}\dfrac{\partial\phi(\mathbf{r}')}{\partial y'}\right)}{|\mathbf{r}-\mathbf{r}'|}dv' \ . \tag{6}$$

We note that the B_x component is the MMR response as defined by Edwards (1974). The TFMMR response is simply the scalar magnetic response,

$$\text{TFMMR} = |\mathbf{B}\cdot\mathbf{f}| \tag{7}$$

where **f** is a unit vector in the direction of the main geomagnetic field.

Electric Potential in Spatial and Wavenumber Domains

In equations (4–6) we require knowledge of the electric potential as a function of position **r'**. The general equation for the electric potential due to a current source in a non-uniform media is given by Poisson's equation

$$\begin{aligned}\nabla^2\phi &= -\rho\,(\nabla\sigma\cdot\nabla\phi + \nabla\cdot\mathbf{J}) \\ &= -\rho\,(\nabla\sigma\cdot\nabla\phi + I\delta(\mathbf{r}-\mathbf{r}_s))\end{aligned} \ , \tag{8}$$

where ρ is the resistivity (=1/σ) (Keller and Frischknecht, 1966). In equation (8) the second term can be viewed as the contribution from a single point current electrode in a uniform half space with resistivity ρ, whereas the first term represents the effect of a charge distribution that accumulates at discontinuities in resistivity, as $\nabla\sigma$ is non-zero only at these places. From this result and the modified Biot-Savart law, we may conclude that both DC resistivity methods and their magnetic versions (MMR, MIP, TFMMR, and TFMMIP) are equivalent and complementary to each other in terms of the parameter sought (resistivity distribution).

For a 2D structure striking in the y-direction with a three-dimensional (3D) point-source electrode, by using the vector identity

$$\nabla\sigma\cdot\nabla\phi = \frac{1}{2}\left(-\sigma\,\nabla^2\phi + \nabla^2(\sigma\,\phi) - \phi\nabla^2\sigma\right) , \tag{9}$$

and substituting in equation (8) we get:

$$\begin{aligned}\nabla^2\{\sigma(x,z)\phi(x,y,z)\} + \sigma(x,z)\nabla^2\phi(x,y,z) \\ -\phi(x,y,z)\nabla^2\sigma(x,z) = -2I\,\delta\,(\mathbf{r}-\mathbf{r}_s)\end{aligned} \tag{10}$$

(Dey and Morisson, 1979).

To arrive at a purely 2D partial differential equation we may remove the y-dependency through a one-dimensional (1D) Fourier transform defined as:

$$\bar{\phi}(x,k_y,z) = \int_{-\infty}^{+\infty}\phi(x,y,z)e^{-ik_y y}dy \ , \tag{11a}$$

$$\phi(x,y,z) = \frac{1}{2\pi}\int_{-\infty}^{+\infty}\bar{\phi}(x,k_y,z)e^{ik_y y}dk_y \ , \tag{11b}$$

where k_y is the wavenumber associated with the y-axis.

Applying equation (11a) to (10), denoting the Fourier transform by FT, and using the derivative property of Fourier transform pairs (Bracewell, 1986), then

$$\mathrm{FT}\left(\frac{\partial}{\partial y}u(x,y,z)\right) = -k_y\bar{u}(x,k_y,z) \ , \tag{12}$$

yields:

$$\frac{\partial}{\partial x}\left(\sigma\frac{\partial\bar{\phi}}{\partial x}\right)+\frac{\partial}{\partial z}\left(\sigma\frac{\partial\bar{\phi}}{\partial z}\right)-\frac{k_y^2}{\rho}\bar{\phi}=-I\,\delta(\mathbf{r}-\mathbf{r}_s)\,. \quad (13)$$

Equation (13) is the 2.5D Helmholtz equation in the wavenumber domain that is solved for a number of k_y values to sample the spectrum of the potential values $\bar{\phi}(x,k_y,z)$ in the wavenumber domain. Because the potential decrease is inversely proportional to the distance from source, then the transformed potential has asymptotic behaviour as the modified Bessel function of zero order since the Fourier transform of the electric potential for a homogeneous Earth model is given as:

$$\mathrm{FT}[\phi(r')]=\mathrm{FT}\left[\frac{\rho I}{2\pi r'}\right]=\frac{\rho I}{2\pi}K_0(k_y r), \quad (14)$$

where

$$r'=\left[(x-x_s)^2+y^2+(z-z_s)^2\right]^{1/2}, \quad (15)$$

and

$$r=\left[(x-x_s)^2+(z-z_s)^2\right]^{1/2} \quad (16)$$

are the radial distances from the source (Snyder, 1976). The coordinate of the current source in the x-z plane is (x_s, z_s), and k_y is the wavenumber corresponding to the y coordinate.

Magnetostatic Formulation in the Wavenumber Domain

After determining the current density distribution (or equivalently the electric potential distribution in equation (13)) due to the current source $I\delta(\mathbf{r}\text{-}\mathbf{r}_s)$, we may use either the general Biot-Savart law (equation (1)) or the modified Biot-Savart law (equation (2)) to compute the associated magnetic field. For computational efficiency we have chosen to formulate the modified Biot-Savart law in wavenumber domain by taking the Fourier transform of the B_x (MMR) component (equation (4)) in the y-direction to obtain the following convolution integral:

$$\bar{B}_x(x,k_y,z)=\frac{\mu_0}{4\pi}\int_0^\infty\int_{-\infty}^\infty\frac{\partial\sigma(x',z')}{\partial z'}dx'dz'\;\mathrm{FT}\left[\int_{-\infty}^\infty\frac{\partial\phi(x',y',z')}{\partial y'}\frac{dy'}{|\mathbf{r}-\mathbf{r}'|}\right]. \quad (17)$$

We use the following identities (Bracewell, 1986):

$$\mathrm{FT}[f(y)*g(y)]=\mathrm{FT}[f(y)]\,\mathrm{FT}[g(y)]\,, \quad (18)$$

and the relationship (Erdélyi et al., 1954):

$$\mathrm{FT}\left[\frac{\partial\phi(x',y',z')}{\partial y'}\right]=-k_y\phi(x',k_y,z'), \quad (19)$$

$$\mathrm{FT}\left[\frac{1}{\left[(x-x')^2+y^2+(z-z')^2\right]^{1/2}}\right]=2\mathrm{K}_0(k_y r')\,, \quad (20)$$

in which

$$r'=\left[(x-x')^2+(z-z')^2\right]^{1/2}, \quad (21)$$

and K_0 is the modified Bessel function of the zeroth kind. By substituting equations (18–21) into equation (14) we obtain the final equation for the B_x (MMR) component in wavenumber domain

$$\bar{B}_x(x,k_y,z)=\frac{-\mu_0}{2\pi}\int_0^\infty\int_{-\infty}^\infty k_y\frac{\partial\sigma(x',z')}{\partial z'}\bar{\phi}(x',k_y,z')\mathrm{K}_0(k_y r')\,dx'dz'\,. \quad (22)$$

Using a similar approach, we find the following expressions for y and z components:

$$\bar{B}_y(x,k_y,z)=\frac{-\mu_0}{2\pi}\int_0^\infty\int_{-\infty}^\infty\left[\frac{\partial\sigma(x',z')}{\partial z'}\frac{\partial\bar{\phi}(x',k_y,z')}{\partial x'}-\frac{\partial\sigma(x',z')}{\partial x'}\frac{\partial\bar{\phi}(x',k_y,z')}{\partial z'}\right]\mathrm{K}_0(k_y r')\,dx'dz', \quad (23)$$

$$\bar{B}_z(x,k_y,z)=\frac{\mu_0}{2\pi}\int_0^\infty\int_{-\infty}^\infty k_y\frac{\partial\sigma(x',z')}{\partial x'}\bar{\phi}(x',k_y,z')\mathrm{K}_0(k_y r')\,dx'dz'\,. \quad (24)$$

Equations (22–24) are the expressions for the magnetic field components in the wavenumber domain. These expressions, along with the electric potential in equation (14), form the basic equations for calculating the components of the magnetic field in wavenumber domain. Once calculated, both the electric potential and the magnetic field components can be determined from an inverse Fourier transform for a range of wavenumbers.

2.5D FORWARD MODELLING SOLUTIONS

The numerical algorithm presented here involves a finite element (FE) approximation to the transformed electric potential over the entire half-space domain for a range of wavenumbers (equation (13)), followed by a set of numerical line integrations of the transformed potentials over the boundaries of the inhomogeneities for each of the three orthogonal anomalous magnetic field components (equations (22–24)). Results in the spatial domain are obtained by taking an inverse Fourier transformation for magnetic fields calculated for a set of strategically chosen wavenumbers. The FE formulation for the transformed electric potential distribution is based on the methods of Wannamaker et al. (1987) and Hohmann (1988).

Figure 2 shows schematically the mesh for a typical TFMMR model. Away from the central region, the element size in both vertical and horizontal directions is increased almost exponentially toward the bottom and side boundaries to satisfy boundary conditions. In methods employing a galvanic current source, there is no need to discretise the air region (upper half space) as there is no conductive current flowing in that region.

An important aspect of 2.5D modelling is appropriate choice of wavenumbers (values of k_y) that properly construct the spectrum of the transformed potential or magnetic fields. Wavenumbers must be strategically chosen so that the effects of aliasing and under-sampling are kept as small as possible, balanced by computational constraints. Because the solution of the system of equations for the transformed electric potential requires the largest fraction of computing time, a number of different approaches for selecting the optimum wavenumber values were attempted. As was shown in equations (13–14), the analytic solution for the transformed potential above a homogeneous half space is simply the modified Bessel function of order zero. Therefore, we must select our spectral sampling points to sample the spectrum of $K_0(k_y r)$ properly.

Unlike DC resistivity modelling, where potential electrodes are almost always set apart from the current electrodes, in TFMMR modelling it is necessary to evaluate the anomalous field even at the position of the current electrodes. This means that the spectrum of the anomalous field components has a wide range of variation corresponding to the distance of the observation point from the current source. This point may be shown by studying the behaviour of the modified Bessel function (Figure 3), which represents the behaviour of the spectrum of a homogeneous half space on the surface of the Earth $z = 0$, given as:

$$\bar{\phi}(x,k_y,z) = \frac{\rho I}{2\pi} \mathrm{K}_0(k_y|x|) \ . \tag{25}$$

Figure 3 shows the behaviour of the modified Bessel function of order zero at different distances from the source. As can be seen from the figure, this function has the following asymptotic behaviour

$$\text{As } k_y|x| \to 0 \text{ then } \mathrm{K}_0(k_y|x|) \to -\ln(k_y|x|) \ , \tag{26}$$

and

$$\text{as } k_y|x| \to \infty \text{ then } \mathrm{K}_0(k_y|x|) \to \left[\frac{\pi}{2k_y|x|}\right]^{1/2} e^{-k_y|x|} \tag{27}$$

(Abramowitz and Stegun, 1972).

Validation and Accuracy

Previous numerical studies using FE or finite difference methods have reported an average of 3–10% error in their approximations (Dey and Morrison, 1979; Pridmore et al., 1981). Here, numerical results for different components of the isotropic homogeneous Earth and vertical fault models are compared to their respective analytic solutions given by Fathianpour and Cattach (1995). It should be emphasised that propagation of errors in calculating the TFMMR response is highly dependent upon the local geomagnetic direction that determines the introduction of errors associated with all three anomalous components. As a result, the TFMMR error would naturally vary between the average error distributed in

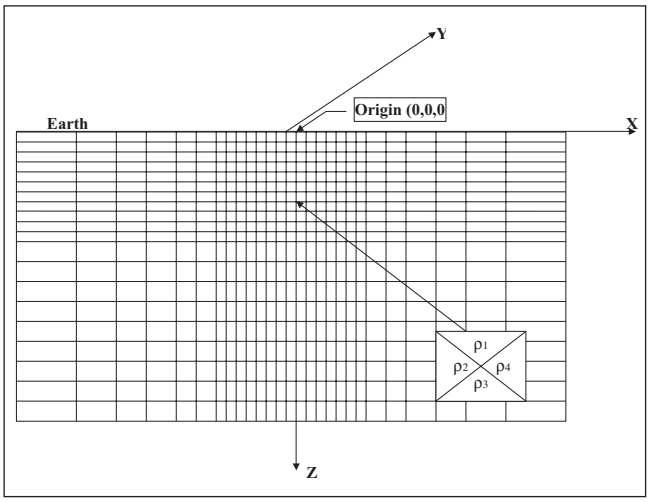

Fig. 2. Section of the FE mesh used in 2.5D forward modelling. Note that each rectangular element is composed of four triangular elements that can be assigned different resistivities as shown in the enlargement.

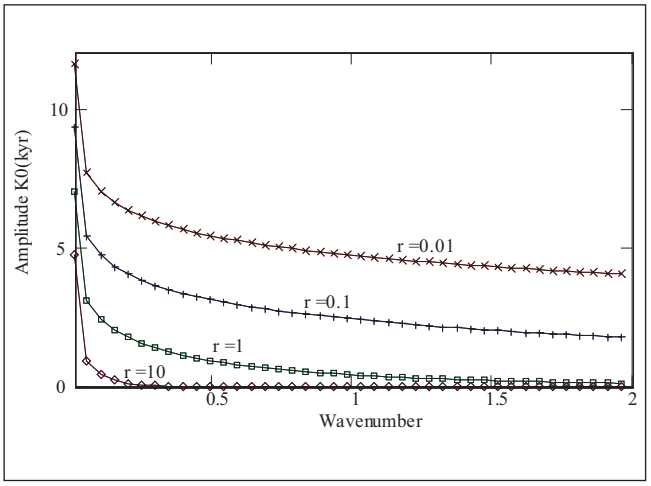

Fig. 3. Behaviour of the modified Bessel function of order zero as a function of distance. The logarithmic singularity at the origin occurs for both electrode location (r = 0) and zero wavenumber.

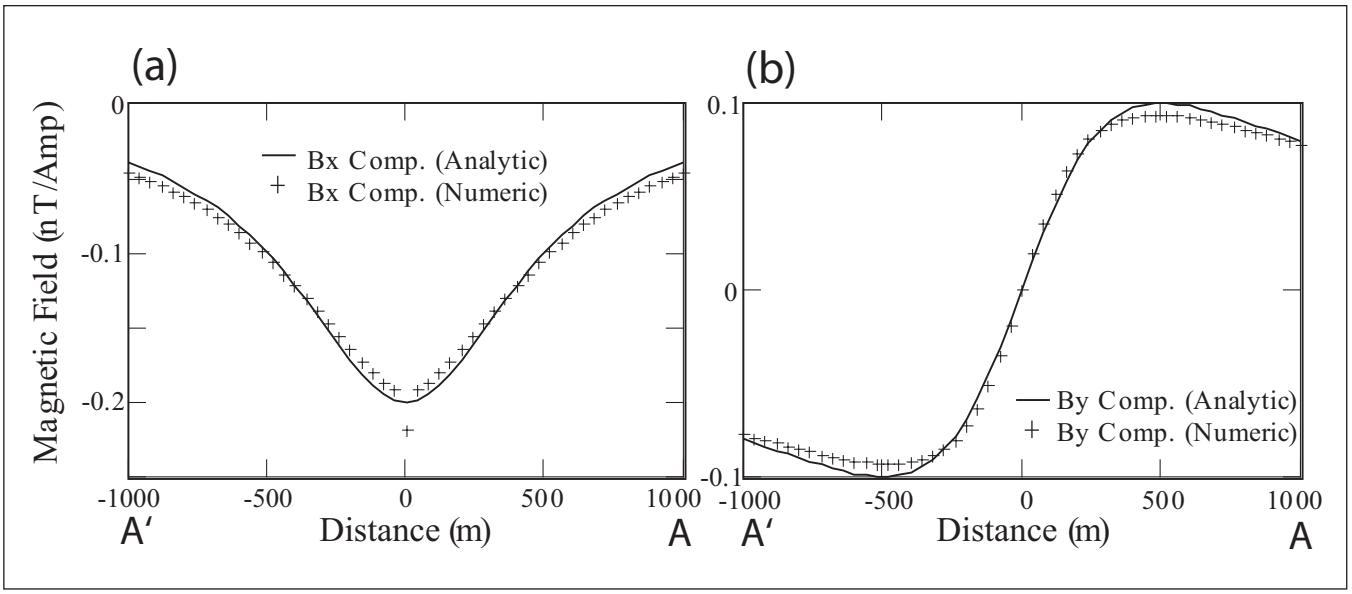

Fig. 4. Comparison of numerical results with corresponding analytical solutions for an isotropic homogeneous half-space for a) the B_x (MMR) component, and b) the B_y component. Results are shown for profile A-A′ in Figure 1 for L = 1000 m, and for one source electrode at the origin.

each component and, depending on the model considered, it may sometimes increases or decrease. Results presented here are for declination of 25° and inclination of 60°, typical of mid-latitudes.

In order to compare the response of different models, a normalised convention was adopted. It was found that normalisation of all scale lengths of the problem to the perpendicular distance joining the measuring profile to the current source electrode has the advantage of both generalising the profile data and providing the ability of producing results for any profile perpendicular to the strike of geological structures and distant L from the current source electrode by simply dividing the normalised values by the profile distance. This is a direct consequence of the similarity theorem of the Fourier transformation (Bracewell, 1986) which states that if $f(y)$ has the Fourier transformation $F(k)$, then $f(ay)$ has the Fourier transformation

$$|a|^{-1} F(k/a) \ . \tag{28}$$

In the case of the magnetic field computation in the wavenumber domain, as all scale lengths are normalised (unit distance becomes the profile distance, L) then the expansion in the space domain scale corresponds to compression of the wavenumber domain scale and vice versa.

Homogeneous Isotropic Test Model

Figure 4 is a plot of the numerical and analytical results for the x and y components of the magnetic field due to a homogeneous half space (i.e., the normal field). The results are for the profile A-A' of Figure 1 by employing only one current source at the origin. A total of 12 wavenumber values were used for approximating the spectrum of the field components in the wavenumber domain. A mesh composed of 40×30 rectangular elements was used, which included a total of 2471 nodes and 4800 triangular elements. As can be seen from Figure 4 the numerical results for the x and y components agree well with analytical results.

For the B_x (MMR) component, the maximum error (9%) occurs at the current electrode location, which may be excluded from error analysis as the solution at this point is simply an interpolation over the singularity, and at the most-distant points from the current source (with maximum relative error of 17% at ±1000 m) where the magnitude of the field decreases rapidly, producing larger round-off errors. However, average B_x error over the whole profile length is 4%.

The accuracy of the B_y component is almost always worse than the B_x component, mainly because of a different spectrum pattern (insufficient wavenumbers) and the extra numeric directional

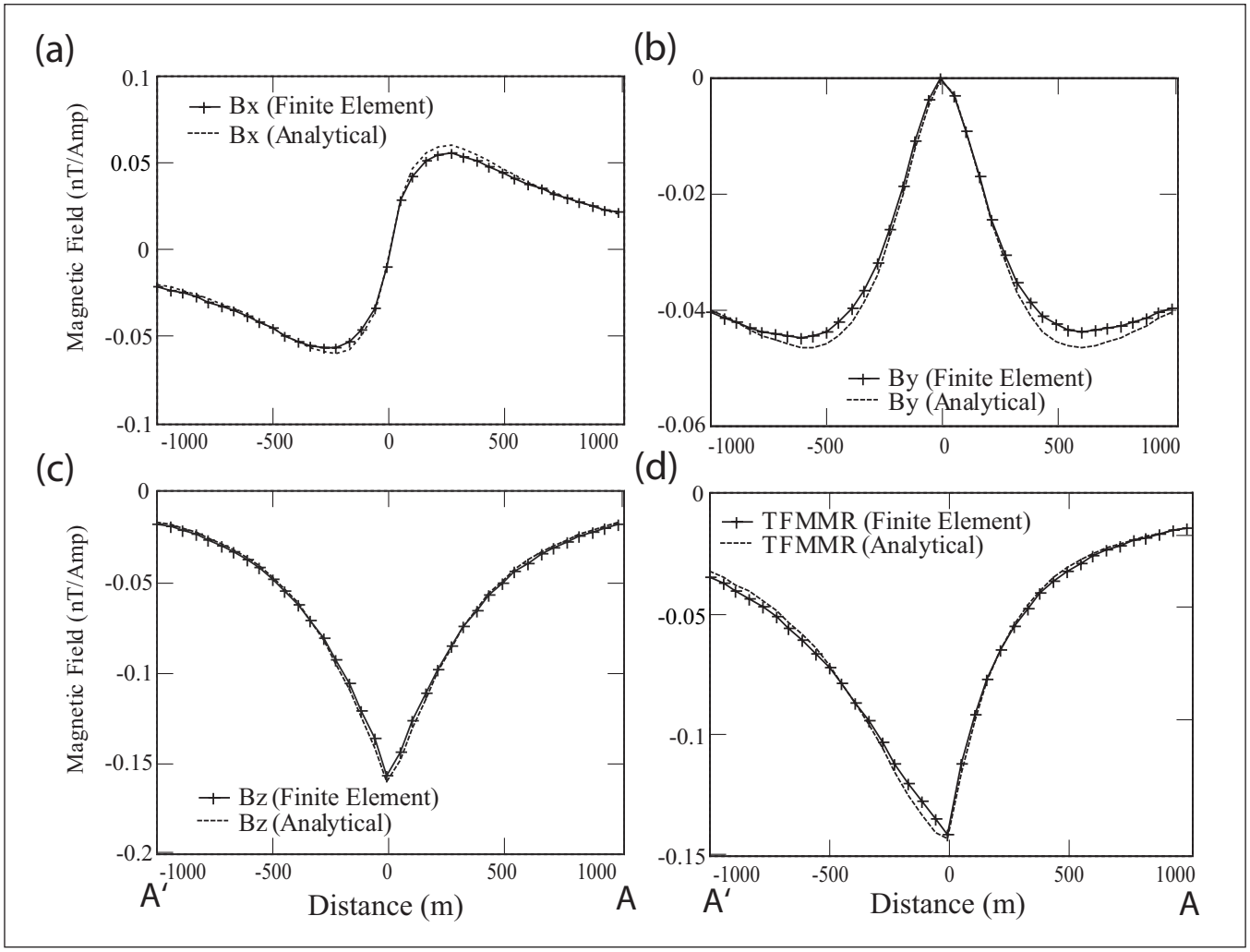

Fig. 5. Comparison of numerical and corresponding analytical solutions for a vertical fault mode for a) the B_x (MMR) component, b) the B_y component, c) the B_z component, and d) the TFMMR response. All results are given for the profile A-A′ of Figure 1 for L = 1000 m and for one source electrode at origin. Note the smaller scale for B_y.

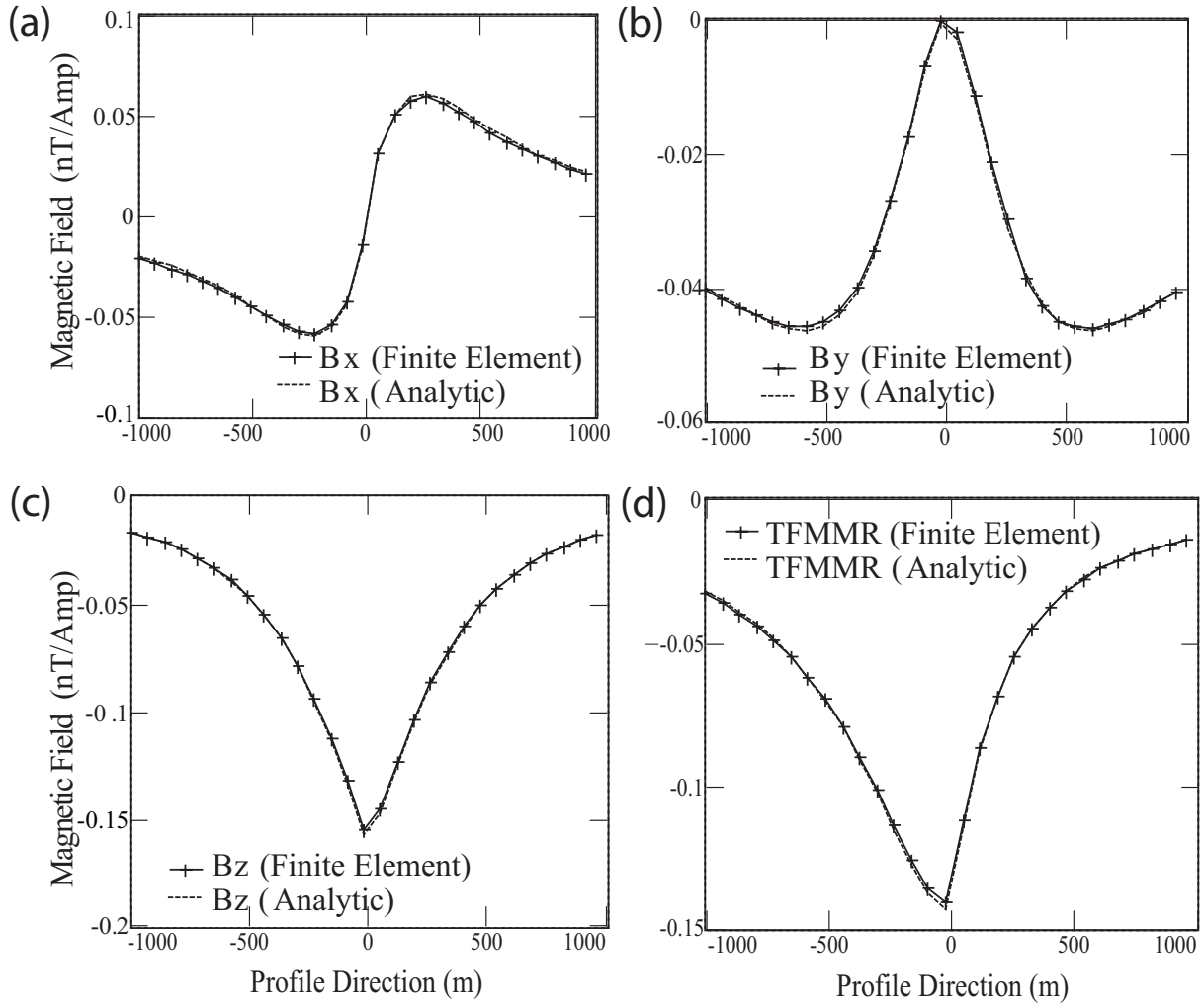

Fig. 6. Comparison between the numerical and analytical results for a vertical fault model. The configuration used here is the same as that for Figures 4 and 5. A larger mesh of 82 × 35 rectangular elements and a set of 40 wavenumbers were used for constructing a) the B_x (MMR) component, b) the B_y component, c) the B_z component, and d) the TFMMR response.

derivative approximations needed in its evaluation. Moreover, the spectrum of the B_y component is indefinite at zero wavenumber and demonstrates a logarithmic singularity near, but not at, $k_y = 0$. Nevertheless, results for the B_y component (average error of 4%) show an excellent match with the analytical results (Figure 4).

Vertical Fault Test Model

Figure 5 demonstrates numerical and analytical calculations of the anomalous magnetic field arising from a vertical fault model with a change in resistivity across the fault of $\rho_2/\rho_1 = 10$. The only current electrode is placed on the trace of the fault on the Earth's surface. The first FE mesh (the coarse mesh) used for this model was composed of 40 × 30 rectangular elements in the x and z directions respectively, using a set of 12 wavenumbers.

From Figure 5, numerical results are in good agreement with the analytical solutions. As for the homogeneous model example, the maximum errors for B_x occur at the tails of the anomalous curve, with an average error of 1.5%. Magnitude of the B_y component is, in general, less than the corresponding analytic result, and occurs at the peak values of the anomalous field at about $x = \pm 500$ m. The numerical B_z component is very close to the true analytical solution, and the maximum errors occur at both ends of profile (about 14%), while the average error is 5%. The TFMMR response has an average relative error of 3%.

To complete this study, the same vertical fault model was modelled with a larger mesh of 82 × 35 rectangular elements, and employed 40 wavenumbers to achieve a higher level of accuracy. Results are shown in Figure 6. As expected, dense sampling of the spectrum reduced the B_y error to less than 1% at the expense of a slight increase for B_x of 2%. The average errors for B_z and TFMMR for this case were 0.3% and 0.5% respectively.

CONDUCTIVE REGOLITH MODELS

One important issue affecting DC electrical methods is the presence of a weathered regolith layer, with thickness from a few centimetres up to a few hundred metres. It is well known that EM methods have limited use in areas of conductive regolith due to the shallow skin-depths. Additionally, surface DC resistivity methods above conductive regolith result in small potential gradients, yielding low signal-to-noise ratios, and can be distorted

by near-surface heterogeneities. Using laboratory scale modelling, Edwards (1974) has shown that measurement of the magnetic field is superior to measuring the corresponding electric field. This is because the magnetic field measured at the surface is not significantly dependent on near-surface resistivity heterogeneities, as the magnetic field is an integral over a volume distribution of current.

In order to evaluate the effect of conductive regolith on MMR and TFMMR data, a complex basement model of conductive vertical structures (such as zones of mineralisation and alteration) in an otherwise uniform host was modelled, with a conductive overburden layer of variable thickness (Figure 7). Resistivity of regolith was set as 10 Ω.m, while the resistivities of the conductive structures and host basement rocks were 30 Ω.m and 100 Ω.m respectively.

Thicknesses of the regolith ranging from 0.05 to 0.5L (where L is defined in Figure 1) were modelled, and the result for the B_x (MMR) and TFMMR profiles are shown in Figures 8 and 9. The presence of a conductive regolith has little effect on the TFMMR responses provided that its conductance (conductivity × thickness) is less than a critical value, allowing current to penetrate the substructure (Gomez-Trevino and Edwards, 1979).

Using the same approach as Edwards and Howell (1976), we define a response parameter α as

$$\alpha = \frac{2 \cdot G}{\sigma_1 \cdot L_e}, \qquad (29)$$

in which G is the regolith conductance, σ_1 is the conductivity of the host medium, and L_e is the current source and sink separation (equal to 4L as defined in Figure 1). The fraction of current penetrating below this conductive regolith with increasing thickness is shown in Table 1 (Edwards and Howell, 1976).

Thus, for a thin conductive regolith with α much less than unity, corresponding to 54% or more current penetration under it, the anomalous TFMMR response clearly shows the underlying double conductive mineral structure. As α increases, or equivalently with less current penetration beneath the regolith, the responses become rapidly weaker. This point is consistent with results obtained by Gomez-Trevino and Edwards (1979).

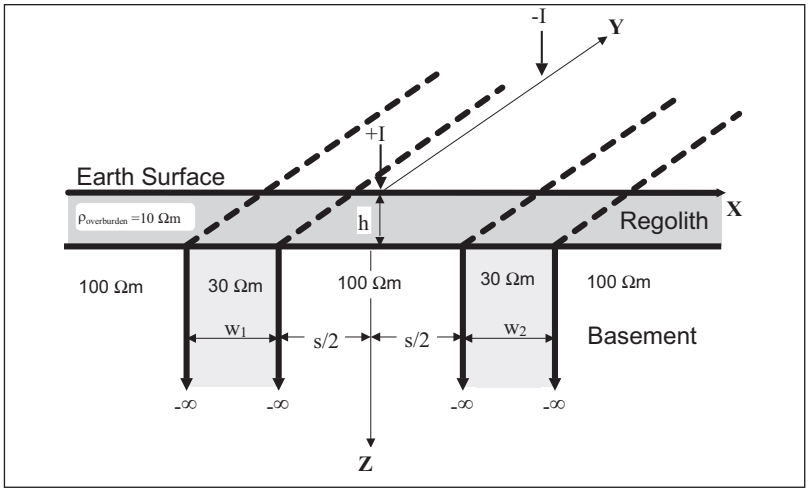

Fig. 7. Geometry of two parallel bedrock conductors beneath a conductive overburden.

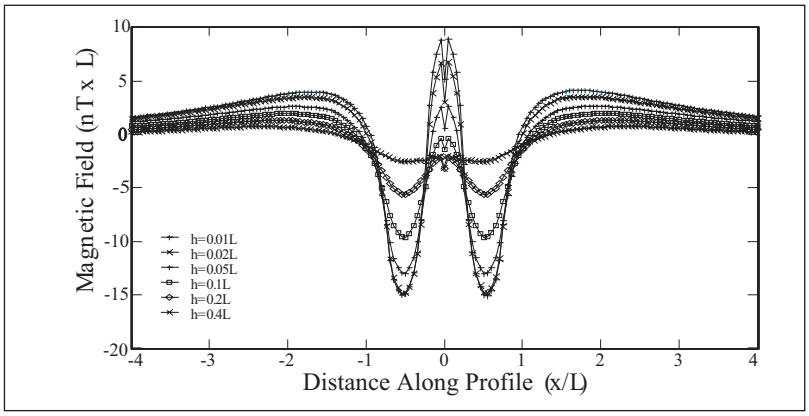

Fig. 8. Effect of regolith thickness on the B_x (MMR) component for the model shown in Figure 7.

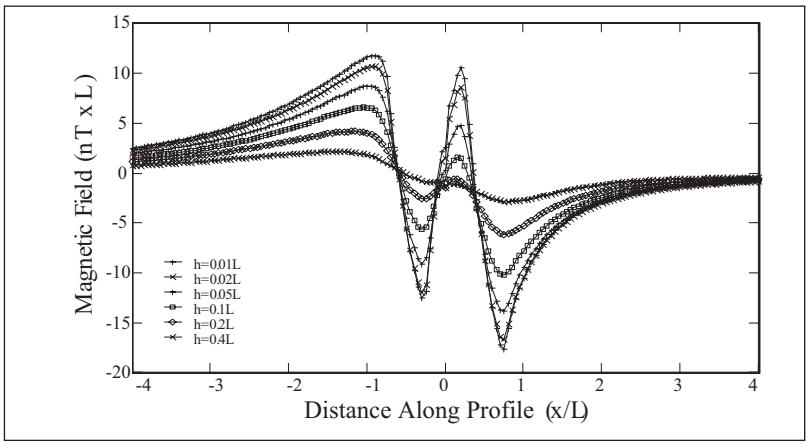

Fig. 9. Effect of regolith thickness on the TFMMR response for the model shown in Figure 7.

Thickness	Regolith Resistivity (Ω.m)	Basement Resistivity (Ω.m)	α	Percentage of current penetrating below regolith
h = 0.01L	10	100	0.05	> 95%
h = 0.02L	10	100	0.1	90%
h = 0.05L	10	100	0.25	77%
h = 0.1L	10	100	0.5	64%
h = 0.2L	10	100	1	54%
h = 0.4L	10	100	2	30%

Table 1. Parameter settings and corresponding percentage current penetrating below conductive regolith.

CONCLUSIONS

A 2.5D numerical forward modelling program has been developed for computing the TFMMR response due to any 2D resistivity structure. In order to achieve the highest accuracy, it was found that a rectangular block comprising four triangular elements is optimal. Using the algorithm, effects of a number of parameters (such as width, thickness, depth and resistivity contrast) of commonly occurring 2D structures with infinite and finite depth extent have been studied. It was found that the peak TFMMR and MMR responses are complicated functions of the depth, thickness, profile distance from the source electrode, and the resistivity contrast with the surrounding host medium.

We have shown that it is possible to derive geometrical and physical parameters of conductive structures beneath a conductive overburden, provided that there is a priori information on the overburden conductance. The anomalous response has a similar spatial wavelength compared to the physical dimensions of the causative body.

ACKNOWLEDGMENTS

We sincerely thank Dr John Stanley and Dr Malcolm Cattach for initial development of the research in the paper during Dr Nader Fathianpour's two-year postgraduate work at the University of New England. At Flinders University, we acknowledge the contributions of Professor S.A. Greenhalgh, Dr F.H. Chamalaun, Mr R. Eames, and Mr A. Moradzadeh. We thank Assoc. Prof. Jayson Meyers and Dr Malcolm Cattach for their constructive reviews that have significantly improved the paper.

REFERENCES

Abramowitz, M., and Stegun, I.A., 1972, *Handbook of mathematical functions with formulas, graphs and mathematical tables.* National Bureau of Standards, 1046p.

Bracewell, R.N., 1986. *The Fourier Transform and Its Applications*. McGraw-Hill, Inc.

Boggs, D.B., Stanley, J.M., and Cattach, M.K., 1999, Three-dimensional numerical modelling of sub-audio magnetic data: *Exploration Geophysics*, **30,** 147–156.

Boggs, D.B., Stanley, J.M., and Cattach, M.K., 1998, Feasibility studies of TFMMIP and TFEM surveying with Sub-Audio Magnetics: *Exploration Geophysics*, **29,** 290–295.

Cattach, M.K., 1996, *Sub-Audio Magnetic (SAM) - A High Resolution Geophysical Method for Simultaneously Mapping Electrical and Magnetic Properties of the Earth*: Ph.D. thesis, University of New England.

Cattach, M.K., Stanley, J.M., Lee, S.J., and Boyd, G.W., 1994, Sub-Audio Magnetics (SAM)- A high resolution technique for simultaneously mapping electrical and magnetic properties: *Exploration Geophysics,* **24**, 387–400.

Dey, A., and Morrison, H.F., 1979, Resistivity modelling for arbitrarily shaped two-dimensional structures: *Geophysical Prospecting,* **27**, 106–136.

Edwards, R.N., 1974, The magnetometric resistivity method and its application to the mapping of a fault: *Canadian Journal of Earth Science,* **11**, 1136–1156.

Edwards, R.N., and Howell, E.C., 1976, A field test of the magnetometric resistivity (MMR) method: *Geophysics,* **41**, 1170–1183.

Edwards, R.N., Lee, H., and Nabighian, M.N., 1978, On the theory of magnetometric resistivity (MMR) method: *Geophysics,* **43**, 1176–1203.

Edwards, R.N., and Nabighian, M.N., 1991, The magnetometric resistivity method. In: Nabighian, M.N. (Ed.), *Electromagnetic Methods in Applied Geophysics. Investigations in Geophysics 3*: Society of Exploration Geophysicists, 47–104.

Erdélyi, A., Oberhettinger, M. F., and Tricomi, F. G., 1954, *Tables of Integral Transforms. Based, in Part, on Notes Left by Harry Bateman and Compiled by the Staff of the Bateman Manuscript Project*: McGraw-Hill.

Fathianpour, N., and Cattach, M.K., 1995, Analytical solutions for the Total Field Magnetometric Resistivity (TFMMR) technique: *Exploration Geophysics,* **26**, 158–166.

Gomez-Trevino, E., and Edwards, R.N., 1979, Magnetometric resistivity (MMR) anomalies of two-dimensional structures: *Geophysics,* **44**, 947–958.

Hohmann, G.W., 1988, Numerical modelling for electromagnetic methods of geophysics. In: Nabighian, M.N. (Ed.), *Electromagnetic Methods in Applied Geophysics,* **1:** Society of Exploration Geophysicists, 313–363.

Keller, G.V., and Frischknecht, F.C., 1966, *Electrical Methods in Geophysical Prospecting*. Pergamon Press, 523pp.

Pridmore, D.F., Hohmann, G.W., Ward, S.H., and Sill, W.R., 1981, An investigation of finite-element modelling for electrical and electromagnetic data in three dimensions: *Geophysics,* **46**, 1009–1024.

Snyder, D.D., 1976, A method for modelling the resistivity and IP response of two-dimensional bodies; *Geophysics,* **41**, 997–1015.

Stanley, J.M., and Cattach, M.K., 1990, The use of high definition mapping in engineering site investigation: *Exploration Geophysics,* **21**, 91–103.

Wannamaker, P.E., Stodt, J.A., and Rijo, L. 1987, A stable finite element solution for two-dimensional magnetotelluric modelling: *Geophysical Journal of the Royal Astronomical Society*, **88**, 277–296.